UC Irvine
UC Irvine Previously Published Works

Title
Electron trapping and acceleration in a modified elongated betatron

Permalink
https://escholarship.org/uc/item/9rs943m9

Journal
Physics of Fluids B: Plasma Physics, 4(11)

ISSN
08998221

Authors
Song, Y.
Fisher, A.
Prohaska, R.
et al.

Publication Date
1992

DOI
10.1063/1.860332

Peer reviewed

eScholarship.org Powered by the California Digital Library
University of California

Electron Trapping and Acceleration in a Modified Elongated Betatron

Y. Song, A. Fisher, R. Prohaska, and N. Rostoker

University of California
Department of Physics, Irvine, CA 92717

ABSTRACT

Electron trapping and acceleration have been successfully accomplished in the modified elongated betatron at U. C. Irvine. About 150 nC of electrons have been trapped and accelerated for ~900 μs until the betatron field reached its maximum, establishing an electron layer with ~80 A of circulating current and ~1.6 MeV of energy in the cylindrical chamber. No minimum current is required to start the beam trapping in the betatron. There are essentially no electron losses during the acceleration at low injection currents; the electron losses at high injection currents are probably caused by the space charge effects, resistive chamber walls, and betatron field ripple. By filling the chamber with plasma, an electron beam of ~120 A current (~230 nC of charge) and ~1.6 MeV energy has been observed. No instabilities have been found during the acceleration except the precessional instability which has been effectively controlled by the toroidal magnetic field. An electron orbit simulation has been carried out, it has shown that practically no resonance instabilities can be developed in the stretched betatron due to its unique geometry and field configuration, which has been confirmed by the experiment.

1. INTRODUCTION

The Purpose of the MEBA[1] (Modified Elongated Betatron Accelerator) is to produce electron beams of high current (kiloamperes) and moderate energy (several to several hundreds of MeV).

The applications of high current accelerators include intense radiation sources from microwaves to X-rays, simulation of nuclear weapon effects, inertial and magnetic confinement fusion, pumping of high power electrically excited lasers and free electron lasers.

The early conventional betatrons are current limited due to space charge during injection. In order to increase beam current, various methods had been tried with little success until a modified betatron was proposed[2,3]. By adding a strong toroidal magnetic field, the space charge limit can be substantially increased in a modified betatron. A 200 A beam had been accelerated to about 1 MeV in the UCI modified betatron[4]. After this, the beam current is further increased by adding a rotating quadrupole field on a modified betatron, this scheme is called a stellatron[5,6]. A 1 kA, 10 MeV beam had been achieved in the UCI stellatron[7]. Recently, a 1 kA beam has been accelerated to about 17 MeV in the NRL modified betatron with a stellarator winding[8].

Unlike a modified betatron or a stellatron which only modifies the magnetic field configuration, the MEBA modifies both the magnetic field configuration and the chamber geometry of a betatron. It has a cylindrical chamber. An axial magnetic field is used as the betatron field to accelerate electrons. This field is of mirror-shape to confine the electrons axially. A toroidal magnetic field is employed to stabilize the electron motion.

Compared with other types of betatrons, the MEBA has the following advantages: 1) Electron injection and trapping are easier to be conducted. 2) It is capable to store more charge and hence has the potentiality of carrying higher currents. 3) Electron confinement is predicted to be more stable. 4) It provides more space and freedom for beam diagnostics and extraction.

With the MEBA, about 150 nC of electrons has been trapped in the evacuated chamber and accelerated until the betatron field reached its peak, giving a ~80 A, ~1.6 MeV circulating beam. By filling the chamber with plasma, a beam of~120 A has been observed.

In Sec. 2 of this paper the basic principles of the MEBA, the simulation of an electron orbit and the analyses of instabilities are presented. In Sec. 3 the apparatus and the diagnostics used in the experiment are described. In Sec. 4 the experimental results are presented along with some interpretations. The experiment is summarized in Sec. 5.

Downloaded From: http://proceedings.spiedigitallibrary.org/ on 01/14/2015 Terms of Use: http://spiedl.org/terms

2. THEORY

The principle illustration of the MEBA is shown in Fig. 1. The accelerator chamber is made of two coaxially mounted pipes. The betatron field is generated by the solenoidal coils, a central solenoid is used to provide the flux to meet the betatron condition. The toroidal field is produced by the current wires along the chamber axis. Electrons are injected at one end of the chamber and trapped in the mirror-shaped betatron field. In the MEBA, electrons follow a helical orbit and bounce back-and-forth axially. Those electrons form a cylindrical electron layer inside the chamber and are accelerated by the increasing betatron field. Fig. 2 shows a typical electron orbit which is plotted from a computer simulation.

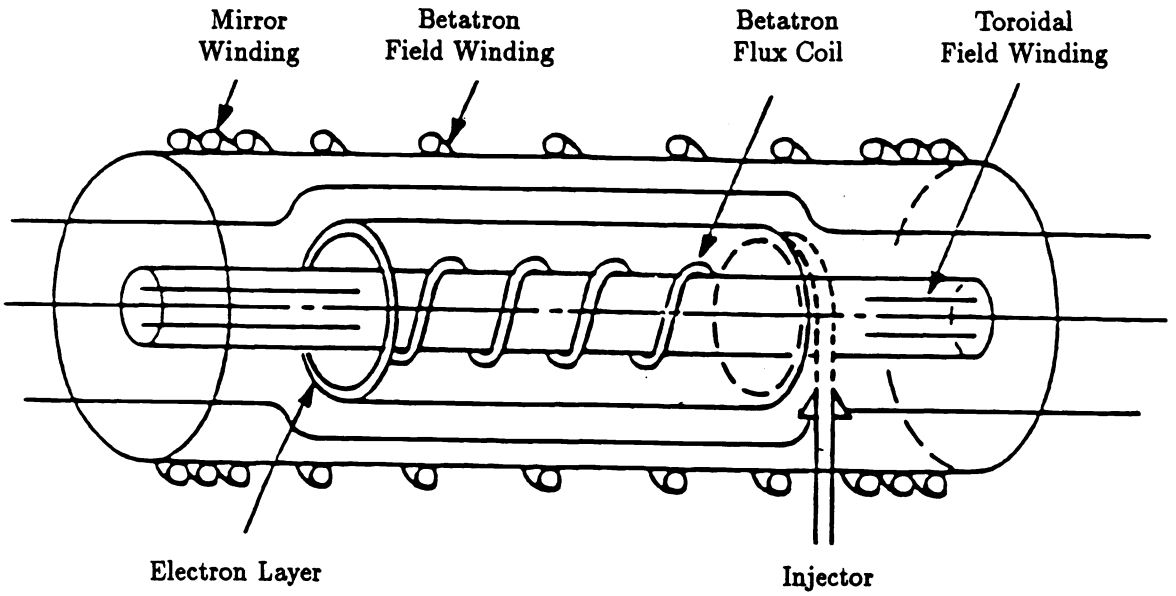

Figure 1. Principle illustration of the MEBA

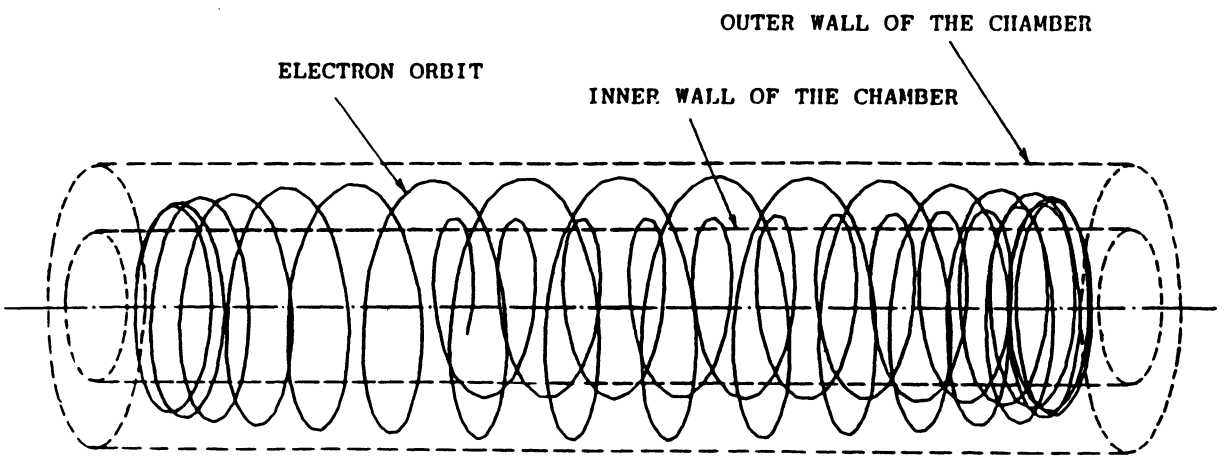

Figure 2. A simulated electron orbit in the MEBA

Downloaded From: http://proceedings.spiedigitallibrary.org/ on 01/14/2015 Terms of Use: http://spiedl.org/terms

2.1. Injection, Trapping and Extraction

The schematic diagram of electron injection and trapping is shown in Fig. 3. The injector is located at one end of the chamber. During injection, the betatron field near the injector is lowered by turning on an "inflector". Due to the mirror configuration of the betatron field,the injected electrons move down to the other end of the chamber and then come back. In the MEBA, the axial oscillation period of an electron is typically 100 ns, which is much longer than the electron gyroperiod in a cyclic accelerator. Therefore one has enough time to turn off the inflector before the electrons come back. Since the magnetic potential near the injector now is higher than that during the injection, the electrons can not reach the injector and are trapped in the mirror field.

When the betatron field reaches its peak, the electrons are accelerated to the maximum energy and have to be extracted. The extraction scheme in the MEBA is shown in Fig. 4. After acceleration, spiller coils are used to compress the electrons to one end of the chamber where the electron radius is expanded and the extraction can be performed.

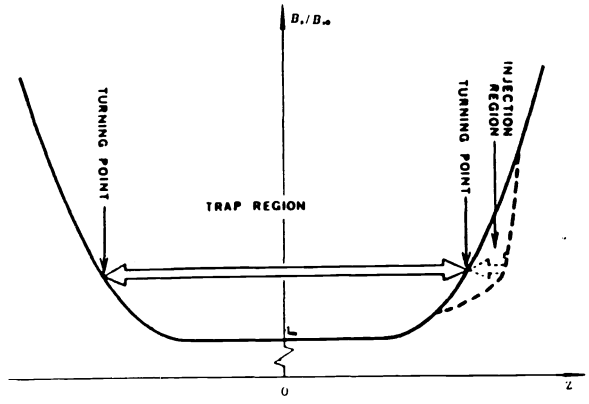

Figure 3. Schematic diagram of beam injection.

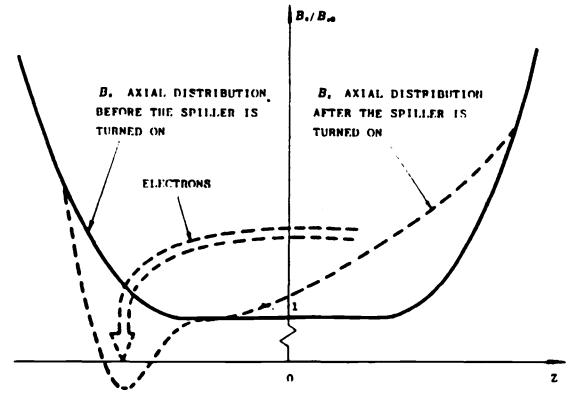

Figure 4. Schematic diagram of beam extraction.

2.2. Space Charge Limits

There are two space charge limits in the MEBA, radial space charge limit and axial charge limit. The radial space charge limit is caused by the so-called Q-oscillation such as those in other types of betatrons. In the MEBA, this space charge limit is

$$n_r \approx \frac{1}{4\pi m_0 \gamma c^2} \left(B_z^2 + B_\theta^2\right) \left(\frac{1}{\gamma^2} - \frac{s}{r_0} \frac{ln\frac{ab}{r_0^2}}{ln\frac{b}{a}} \right)^{-1}$$

where n_r is the electron density, m_0 the electron rest mass, γ the relativistic factor, c the speed of light in vacuum; B_z and B_θ are the betatron and the toroidal field, s and r_0 the half thickness and the average radius of the electron layer, a and b the inner radius and outer radius of the chamber, respectively. For $\frac{s}{r_0} \to 0$

$$n_r \approx \frac{\gamma}{4\pi m_0 c^2} \left(B_z^2 + B_\theta^2\right)$$

The axial space charge limit represents the energy conservation of an electron confined in a mirror field. It can be written as

$$\lambda_a \approx \frac{\gamma^2 - 1}{\gamma} \frac{e}{4r_e} \frac{ln\frac{b}{a}}{ln\frac{r_0}{a} ln\frac{b}{r_0}} \eta$$

where λ_a is the linear charge density, e the elementary charge, r_e the classical electron radius, η the mirror ratio of the betatron field at the injector.

Downloaded From: http://proceedings.spiedigitallibrary.org/ on 01/14/2015 Terms of Use: http://spiedl.org/terms

2.3. Orbital Oscillations

In the MEBA, the electron orbit is less localized and more complicated than those in other types of betatrons therefore it is difficult to analyze. In order to show the characteristics of the electron motion, a computer simulation has been performed. In the simulation, the trajectory of an electron is traced during acceleration. The time-dependent magnetic and electric fields are calculated from the current distribution given by the experimental parameters. A typical electron orbit is shown in Fig. 2. One can see from the figure that the electron gyrates around the chamber axis and at the same time bounces back-and-forth axially. The orbit radius keeps changing with the electron moving axially, this is caused by the Lorentz force of the toroidal field on the electron; the radius is lager when the electron moves axially one way than another. The orbit radius as a function of axial coordinate at three different toroidal field strengths are shown in Fig. 5. It can be seen that a stronger toroidal field causes a larger radial separation of the electron orbit. It can also be seen that the electron oscillates radially about its equilibrium orbit.

One important phenomenon found in the simulation is that the electron orbit in the MEBA is essentially non-periodic. This implies that orbital resonances can not develop in the MEBA. Fig. 6 shows two different electron trajectories over 1 μs simulation. Fig. 7 shows the electron radial oscillation trajectory over 3 μs. The non-periodicity of the electron motion in the MEBA can be seen in these figures. The time dependences of $n_{c,f}$, $n_{r,f}$, $n_{c,b}$ and $n_{r,b}$ are shown in Fig. 8. Here n_c and n_r are the numbers of the gyration and radial oscillation cycles executed by an electron during its one axial trip. The second supscripts f and b represent the cases when the toroidal field is clockwise and anticlockwise relative to the axial motion of the electron, respectively. All these four numbers have to be integers for the orbit to be periodic. Hence Fig. 8 again shows the non-periodicity of the orbit.

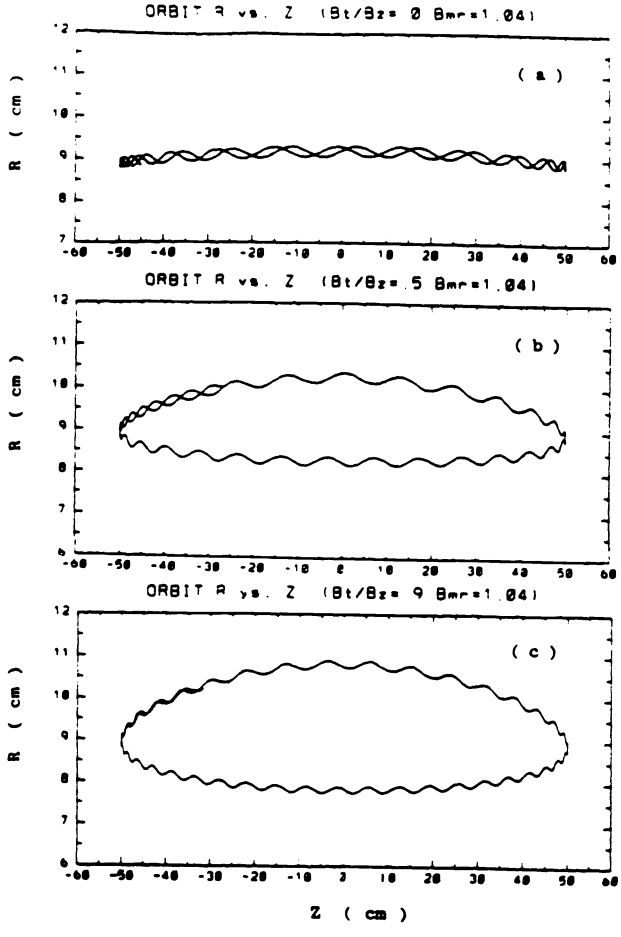

Figure 5. Radial separation and oscillation of the electron orbit at different toroidal field strengths.

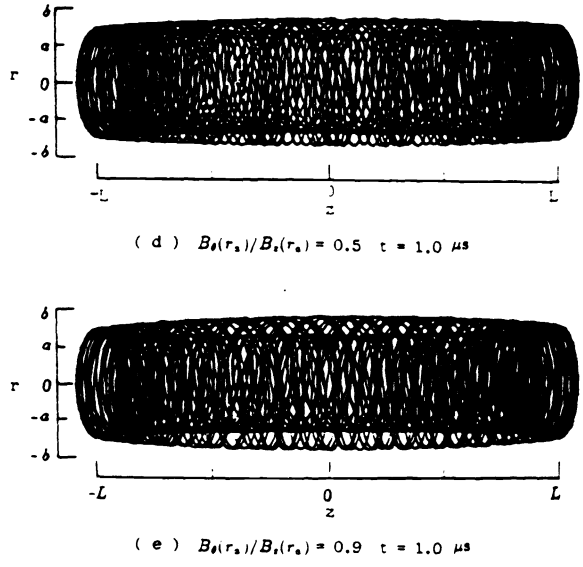

Figure 6. Electron trajectories at two different toroidal field strengths, 1 μs simulation.

Downloaded From: http://proceedings.spiedigitallibrary.org/ on 01/14/2015 Terms of Use: http://spiedl.org/terms

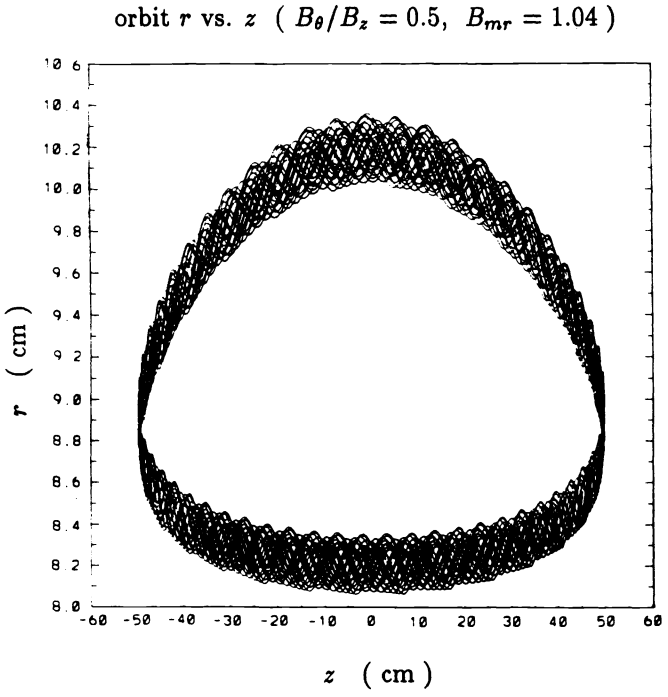

Figure 7. Trajectory of the electron radial oscillation, 3 μs simulation.

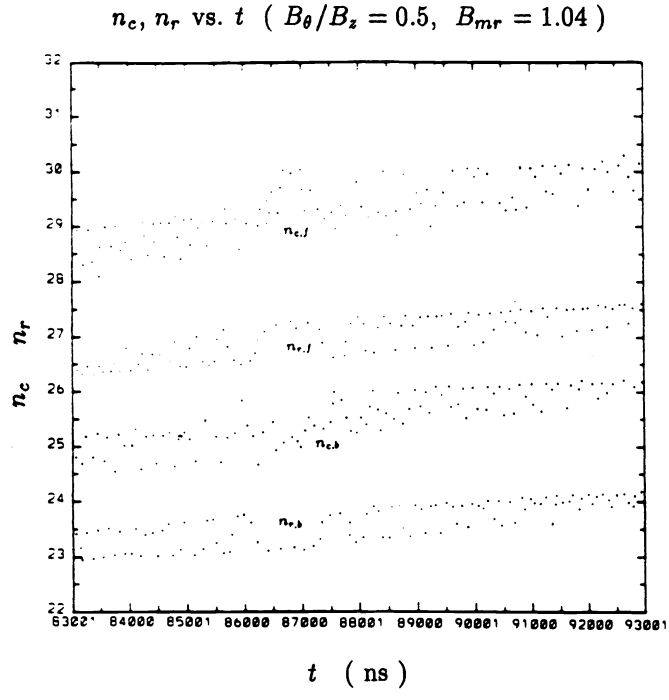

Figure 8. Time dependences of the gyration and radial osillation cycles executed by an electron during its one axial trip.

2.4. Instabilities

The prevalent instabilities in a modified betatron or a stellatron are resonance instabilities[9,10] and negative mass instability[11–14]. According to the simulation above, resonance instabilities are not likely to exist in the MEBA because electron orbit is non-periodic. The experiment in the MEBA has proved this statement: no resonance instabilities were found during acceleration. Neither has the experiment shown any evidence of negative mass instability although the cold electron energy threshold of this instability has been passed. The possible explanations of this are the following. 1) The MEBA has a conductive cylindrical chamber, this kind of geometry can stabilize negative mass modes[15]. 2) The experimental results shows that the MEBA can tolerate relatively large momentum mismatching. The negative mass instability can not grow because of Landau damping[16].

For electrons gyrating in a system with mirror-shaped magnetic field, there is another prevalent instability—precessional instability[17–20]. Precessional instability has been found in the MEBA experiment when toroidal field was absent or very weak. With a relatively strong toroidal field, precessional instability could be effectively suppressed. This result is consistent with that of the Astron experiment[18,20]

3. EXPERIMENTAL SET-UP

3.1. Apparatus

The MEBA was built in the beam laboratory at U. C. Irvine. Fig. 9 is a schematic drawing of the MEBA, and Table I summarize the major parameters of the apparatus.

The vacuum chamber consists of two coaxially mounted glass pipes. The space between the pipes is sealed with Lexan end flanges containing ports. It is evacuated with a diffusion pump. The inner surfaces of the chamber are coated with molybdenum, to make the chamber conductive electrically but transparent magnetically.

Downloaded From: http://proceedings.spiedigitallibrary.org/ on 01/14/2015 Terms of Use: http://spiedl.org/terms

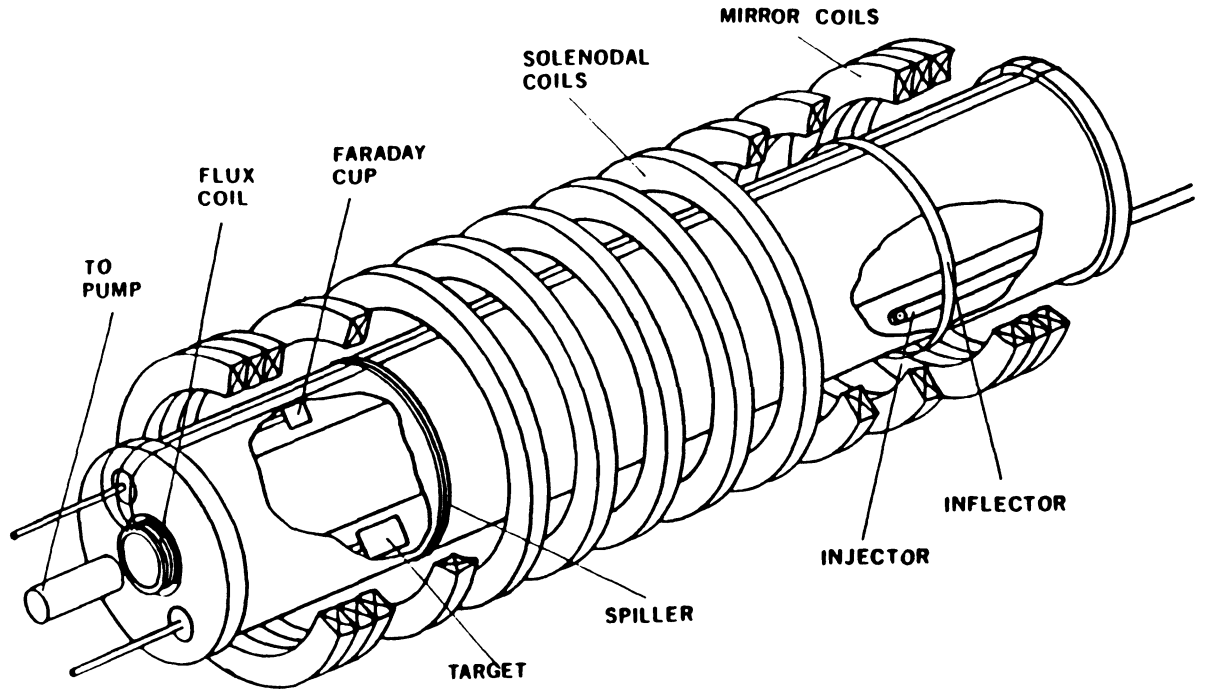

Figure 9. Schematic diagram of the MEBA

TABLE I. Major Parameters of the MEBA

Vacuum chamber	
Length	160 cm
Inner radius	5.8 cm
Outer radius	11.8 cm
Wall resistivity	1.2 $k\Omega$/square
Vacuum	1×10^{-3} — 2×10^{-5} Torr
Betatron field	
Risetime	1 ms (from 0 to peak)
Peak field	750 Gauss
Field ripple	~1% (at $r_0 = 8.8$ cm)
Toroidal field	
Risetime	0.7 — 1.5 ms (from 0 to peak)
Relative strength	$B_\theta/B_z = 0 \sim 2$ (at $r_0 = 8.8$ cm)
Electron injector	
Voltage	30 — 60 kV
Current	0 — 100 A
Pulse width	~100 ns (FWHM)
Inflector	
Falltime	~50 ns (from peak to 0)
Current	0 — 300 A
Width	> 3 μs
Spiller	
Risetime	10 — 15 μs
Peak current	4 — 6 kA

Fourteen solenoidal coils together with the central solenoid produce the axial betatron field and the magnetic flux needed for the acceleration. The closer spaced solenoidal coils at both ends of the chamber form a mirror field configuration. The current in the solenoidal coils is obtained by discharging a capacitor bank. The central solenoid is connected to the secondary winding of a transformer, the primary winding of the transformer is in series with the solenoidal coils. This facilitate control of the current in the central solenoid and so of $\bar{B}_z/B_z$. Here, B_z is the local betatron field strength at the electron orbit and $\bar{B}_z$ is the average betatron field inside the electron orbit. The spatial distribution of the betatron field is shown in Fig. 10. The toroidal field is provided by 36 turns of wire wound around the chamber and threaded between the inner glass pipe and the central solenoid.

The electron injector is shown in Fig. 11. A field emission cathode of graphite fibers is used[21]. Various types of anodes were used during the experiment to change the amplitude and density of the injected current. The operating voltage up to 60 kV is delivered to the injector diode through a 50 Ω Blumlein transmission line. Electrons are injected tangentially into the chamber.

Downloaded From: http://proceedings.spiedigitallibrary.org/ on 01/14/2015 Terms of Use: http://spiedl.org/terms

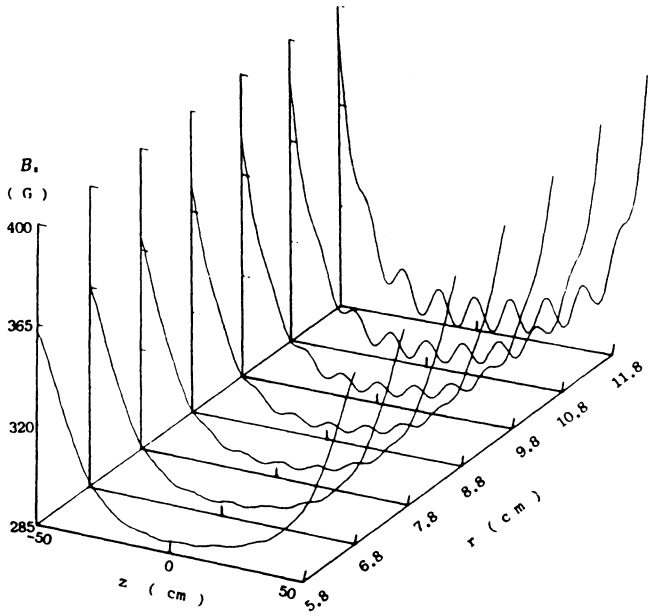

Figure 10. Spatial distribution of the betatron field.

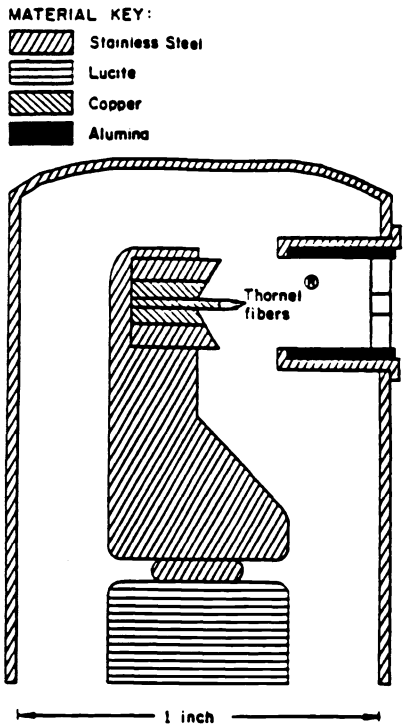

Figure 11. Cross section of the injector used in the MEBA.

The inflector is a single turn loop made of a strip of stainless steel. The current in the inflector is obtained by discharging a capacitor bank and turned off by a hydrogen thyratron. The spiller winding is directly wound on the outer glass pipe. The turns and the location of the winding are adjustable to achieve optimum extraction.

3.2 Diagnostics

The diagnostics of the experiment included pulse current transformers, $\dot{B}$-loops, Faraday cups, X-ray detectors, Phosphor detectors, a voltage divider, and a pinhole camera.

The pulse current transformers were used to measure the currents in the inflector, spiller, and the coils generating the magnetic fields. The $\dot{B}$-loops were used to measure the magnetic field distribution.

Several types of X-ray detectors were used to monitor the X-rays produced when the electron hit the chamber walls, the injector or a target inserted in the chamber. NaI(Tl) or NE-102A plastic scintillators attached to a photomultiplier tube had been used regularly during the experiment. A X-ray pinhole camera was used to locate the source of X-rays along with an array of radiation dosimeters. The injector voltage was monitored by a voltage divider. The Faraday cups, combined with the current probes and X-ray detectors, were used to measure the injected and extracted beam currents.

The phosphor detectors included a phosphor target, a phosphor probe, and a phosphor camera. The phosphor target was a sheet of stainless steel coated with electronic phosphor; the phosphor probe was a piece of optical fibre, coated with phosphor on one end and attached to a photomultiplier tube on another end. They were used to observe the electron distribution after injection. The phosphor camera was used to measure the beam emittance. In this case, the beam first passed a lead grid and then hit a sheet of glass coated with phosphor, the light spots were reflected to a high speed camera by an optical prism.

Downloaded From: http://proceedings.spiedigitallibrary.org/ on 01/14/2015 Terms of Use: http://spiedl.org/terms

4. EXPERIMENTAL RESULTS AND DISCUSSION

4.1. General features

The time sequence of the MEBA operation is the following. Usually the toroidal field wad activated first. The betatron field was delayed from the start of the toroidal field by 0 — 120 μs. Electrons were injected at a proper betatron field strength. When the betatron field reached its peak, the electrons were ejected to the outer wall of the chamber by firing the spiller. The X-rays produced by the beam electrons were monitored throughout the operation, which gave the information about the electron losses during the injection and the acceleration, and the electron charge at the ejection time. The details about the injection and trapping process, the acceleration in both vacuum and in plasma, and the dependence of electron losses on the experimental parameters are discussed hereafter.

4.2. Injection and trapping

Fig. 12 shows the injection and trapping procedure, where a typical time sequence of the injector voltage, the injector emission current, and the cut-off of the inflector current is plotted. The inflector was turned on when the betatron field reached to a certain value at which the gyroradius of the injected electrons was roughly equal to the average radius of the chamber. About 3 μs later, the injector was activated. The inflector was turned off after the injection.

During the experiment, the peak of the toroidal field, the delay of the betatron field relative to the toroidal field, the injection time, and the voltage applied on the inflector were all freely adjusted to optimum the injection and trapping. The X-ray yields at the extraction time as the functions of the above parameters are shown in Fig. 13 — 16. It has been found that good injection and trapping could be performed in a wide range of the experimental parameters.

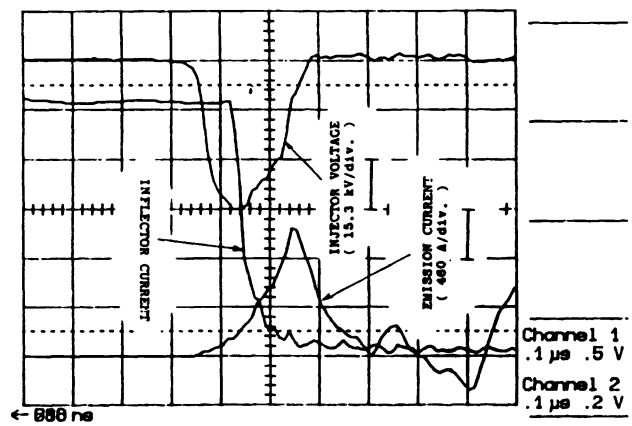

Figure 12. Time sequence of the injector voltage, the injector emission current, and the inflector current.

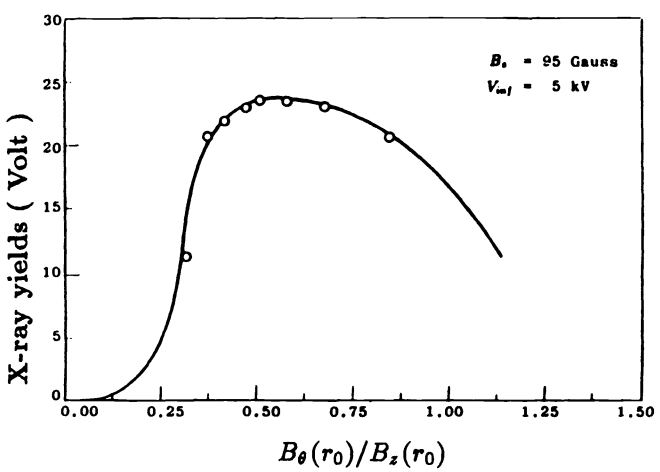

Figure 13. X-ray yields at the extraction time as a function of $B_\theta(r_0)/B_z(r_0)$.

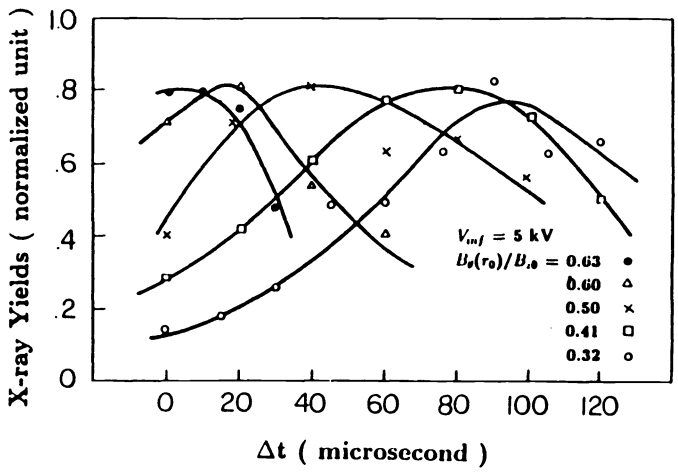

Figure 14. X-ray yields at the extraction time as a function of the delay between B_z and B_θ.

Downloaded From: http://proceedings.spiedigitallibrary.org/ on 01/14/2015 Terms of Use: http://spiedl.org/terms

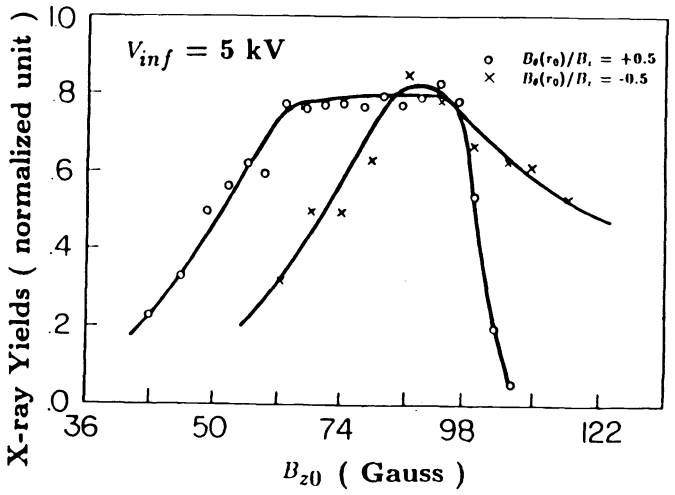

Figure 15. X-ray yields at the extraction time as a function of $B_z(r_0)$ at the injection time.

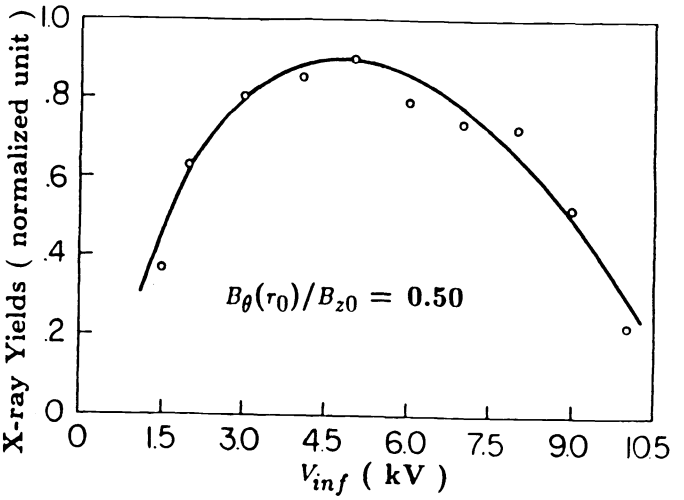

Figure 16. X-ray yields at the extraction time as a function of the inflector voltage.

It has also been found that in the MEBA a beam of arbitrarily low current can be trapped. This means that no collective effects were involved in the injection and trapping procedure. The X-ray yields at different injection currents are shown in Fig. 17.

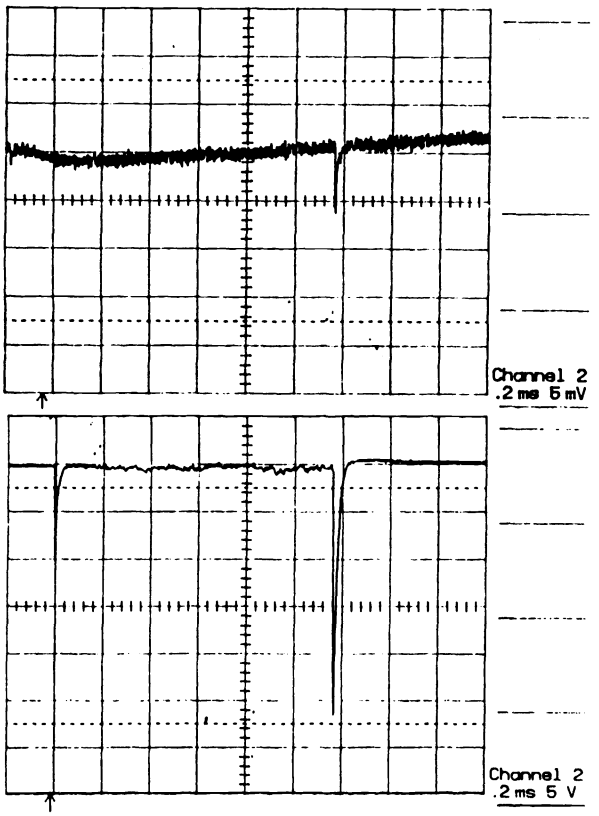

Figure 17. X-ray yields at the extraction time for different injection currents.

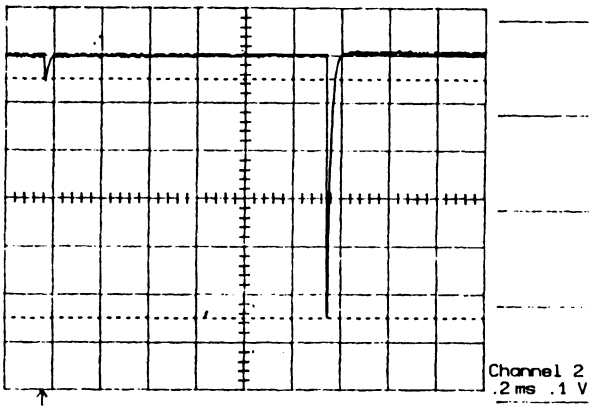

Another phenomenon found in the experiment is that more electrons were trapped when the toroidal field was positive. The toroidal field B_θ is signed positive when it is clockwise seen in the direction of the betatron field. The fine structure of the X-ray yields at the extraction time for $B_\theta > 0$ and $B_\theta < 0$ are shown in Fig. 18. A reasonable explanation of the above phenomenon cab be drawn from the computer simulation mentioned earlier. According to the simulation, when $B_\theta > 0$ an electron spends shorter time near the injector than it does when $B_\theta < 0$, therefore it has less chance to hit the injector and is easier to be trapped.

Downloaded From: http://proceedings.spiedigitallibrary.org/ on 01/14/2015 Terms of Use: http://spiedl.org/terms

4.3. Acceleration in vacuum

When the injection current was low ($I_{inj} < 20$ A), there were essentially no electron losses during acceleration. Fig. 19 shows the X-ray yields in the whole procedure of one shot. It can be seen that there are almost no X-ray yields except during injection and ejection. This fact implies that there are no resonance instabilities in the MEBA, which is consistent with the earlier simulation result.

At higher injection currents ($I_{inj} > 20$ A), some electron losses appeared during acceleration, and trapping efficiency started to decrease because more electrons were lost during injection and trapping. When the injection current was about 50 A, the beam current reached its maximum ~80 A, equivalent to about 150 nC of electron charge. When the injection current was higher than 50 A, the beam current start to decrease very quickly due to the dramatic drop of the trapping efficiency. Almost no X-rays were observed about one microsecond after injection when the injection current was beyond 60 A. The beam current I_b, calculated from the X-ray yield at the extraction time, as a function of the injection current is shown in Fig. 20 (the solid curve).

Although the reasons of causing the electron losses during injection and trapping at high injection currents have not been fully understood, two possible explanations are the high resistivity of the chamber walls and the space charge effects near the injector.

The resistivity of the molybdenum layer coated on the vacuum sides of the chamber is about 1.8 kΩ/square. Due to this high resistivity, the electrons lost on the chamber walls could develop a voltage drop up to tens of kilovolts along the chamber at high injection currents. The voltage drop could cause a major perturbation to the electron trapping and confinement.

In order to reduce the resistivity, stainless steel screens were used to cover the inner surfaces of the chamber in the later period of the experiment.On the screen covered on the inner surface of the outer wall, an axial split of about 1 cm wide was opened all the way along the chamber, to ensure that the outer wall of the chamber was transparent to the betatron field produced by the solenoidal coils.

The dashed curve in Fig. 20 shows the beam current vs. the injection current after the stainless steel screens were installed. In this case, the upper limit of the injection current for electron trapping and beam formation was moved, but more electron losses appeared during acceleration. The maximum beam current is still ~80 A.

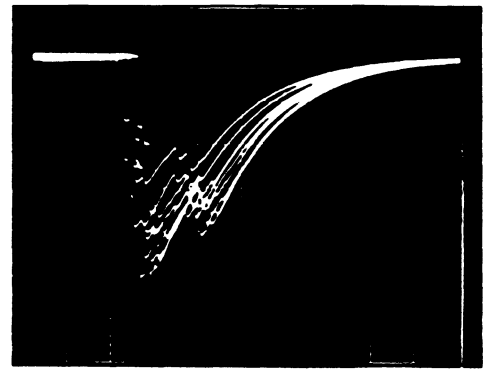

(a) $B_\theta > 0$

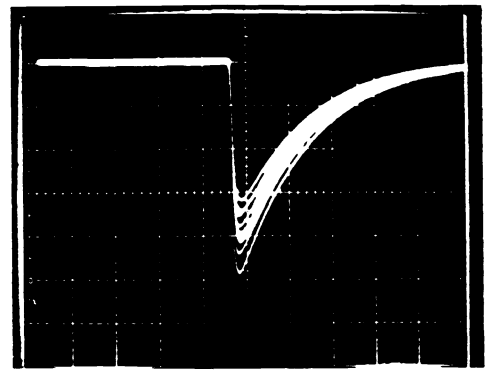

(b) $B_\theta < 0$

Figure 18. Fine structures of the X-ray yields at the extraction time for $B_\theta > 0$ and $B_\theta < 0$. Several shots were taken in each picture.

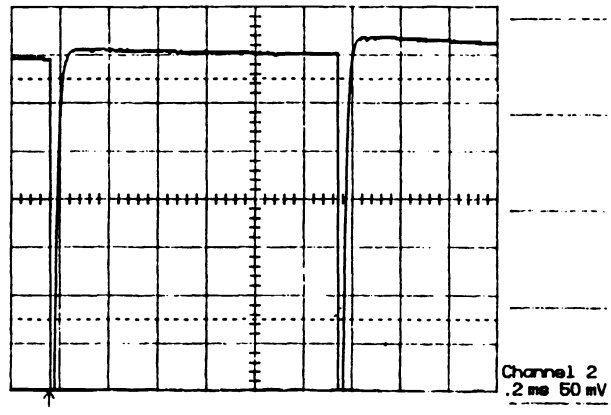

Figure 19. X-ray yields during the injection, acceleration, and extraction in vacuum.

Downloaded From: http://proceedings.spiedigitallibrary.org/ on 01/14/2015 Terms of Use: http://spiedl.org/terms

4.4. Acceleration in plasma

To check the space charge effects in the MEBA, the electron injection, trapping, and acceleration have also been conducted in plasma. One plasma gun was installed on each end of the chamber. A 1/4 inch diameter rigid coaxial cable was used as a plasma gun. The plasma was produced by surface flashover[22]. The power source was a 0.01 — 0.1 μF capacitor, which was charged at 2 — 7 kV and discharged through a hydrogen thyratron. The plasma density near the injector was 10^{11} — 10^{12} cm^{-3}. The optimum beam trapping was observed when the plasma was injected 5 — 15 μs prior to the electron injection. With the plasma injection, the beam current as a function of the injection current is also shown in Fig. 20 (the dotted curve). Compared with the case in vacuum, the maximum beam current increased about 50%. About 230 nC of electrons have been accelerated until the extraction time, giving a ~120 A and ~1.6 MeV circulating electron beam.

Fig. 21 shows the X-ray yields during acceleration with the plasma injection and with the stainless steel screens installed in the chamber. It shows that many electrons were lost on the chamber walls during acceleration. The causes of these losses are probably the following: the non-symmetry of the system introduced by the screens, plasma instabilities, and the ripple of the betatron field. The last factor has been checked during the experiment; by increasing the field ripple from 1% to 2%, the beam current decreased about one order.

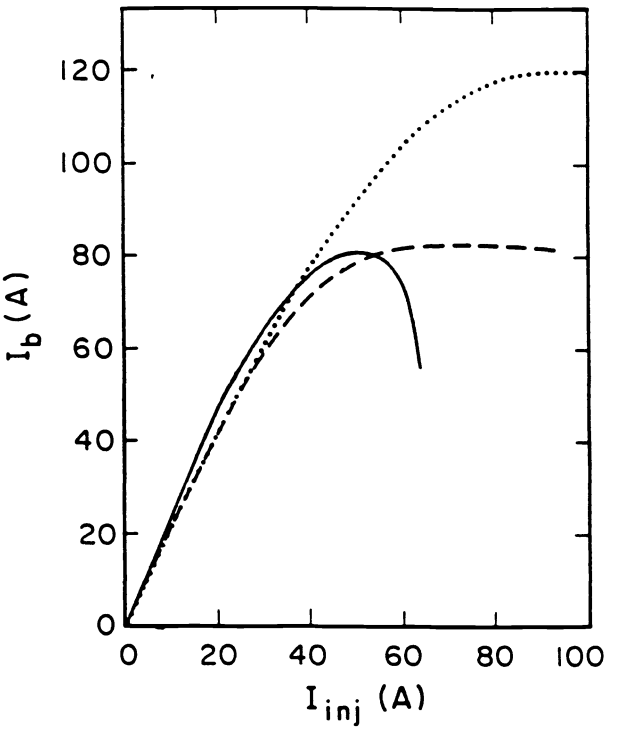

Figure 20. Dependence of beam current on the injection current in 1) the evacuated chamber (solid curve), 2) the evacuated chamber with the screen liner (dashed curve), and 3) the plasma filled chamber with the screen liner (dotted curve).

5. SUMMARY

In this work the electron injection, trapping, and acceleration in the MEBA have been investigated both theoretically and experimentally. An electron beam of ~80 A of current and ~1.6 MeV of energy has been observed. With plasma injection, the beam current increased to about 120 A. These results has shown the potentiality of using the MEBA as a high current accelerator.

In principle the injection and trapping can be easily accomplished in the MEBA. The experimental results has also shown that a beam can be formed in a wide range of experimental parameters. No minimum current is required to start trapping, this means that no collective effects are involved in the beam formation. Therefore the MEBA can be also used to generate low current electron beams which are useful in channeling radiation.

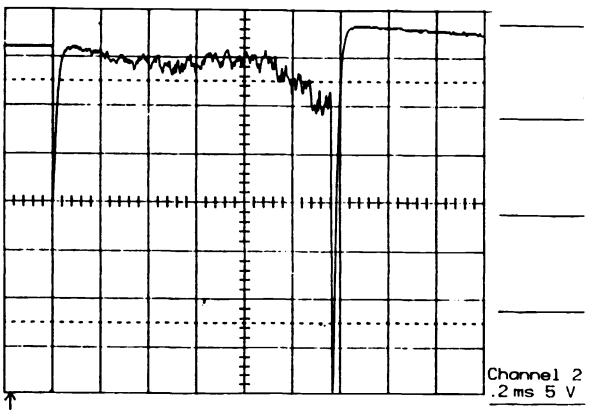

Figure 21. X-ray yields during the injection, acceleration, and extraction in plasma.

In vacuum, the beam current is limited probably by the high resistivity on the inner surfaces of the chamber and the space charge effects near the injector. In plasma, the electron losses during acceleration are probably caused by the plasma instabilities, the ripple of the betatron field, and some other factors.

Downloaded From: http://proceedings.spiedigitallibrary.org/ on 01/14/2015 Terms of Use: http://spiedl.org/terms

Further studies are needed in order to understand the mechanism that causes the electron losses and limits the beam current. More experiments, such as modifying the magnetic field configuration and reducing the ripple of the betatron field, are also necessary to increase the beam current.

5. ACKNOWLEDGMENTS

This paper is based on the work that was done during 1987 — 1989 and on the Ph. D. dissertation submitted by Y. Song to the University of California, Irvine. The assistance of the colleagues in the UCI Beam Lab is greatly appreciated.

6. REFERENCES

1. A. E. Blaugrund, A. Fisher, R. Prohaska, and N. Rostoker, *J. Appl. Phys.* **57**, 2474 (1985)
2. P. Sprangle and C. A. Kapetanakos, *J. Appl. Phys.* **49**, 1 (1978)
3. N. Rostoker, *Comments Plasma Phys. and Controlled Fusion* **6**, 91 (1980)
4. H. Ishizuka, G. Lindley, B. Mendelbaum, A. Fisher, and N. Rostoker, *Phys. Rev. Lett.* **53**, 266 (1984)
5. C. W. Roberson, M. Mondelli, and D. Chernin, *Phys. Rev. Lett.* **50**, 507 (1983)
6. C. W. Roberson, M. Mondelli, and D. Chernin, *Particle Accelerators* **17**, 79 (1985)
7. H. Ishizuka, J. Saul, A. Fisher, and N. Rostoker, *Proc. of 6th Intl. Conf. on High Power Particle Beams*, June 1986, Kobe, Japan, p. 722
8. L. K. Len, T. Smith, J. Golden, S. J. Marsh, D. Dialetis, J. Mathew, P. Loschialpo, J. H. Chang, and C. A. Kapetanakos, *Bull. Am. Phys. Soc.* **35**, 2073 (1990)
9. D. Chernin and P. Sprangle, *Particle Accel.* **12**, 101 (1982)
10. G. Barak and N. Rostoker, *Phys. Fluids* **26**, 856 (1983)
11. R. W. Landau and V. K. Neil, *PHys. Fluids* **9**, 2412 (1966)
12. R. W. Landau, *Phys. Fluids* **11**, 205 (1968)
13. R. C. Davidson and H. S. Uhm, *Phys. Fluids* **25**, 2089 (1982)
14. G. Roberts and N. Rostoker, *Phys. Fluids* **29**, 333 (1986)
15. R. J. Briggs and V. K. Neil, *plasma Phys.* **8**, 255 (1966); **9**, 209 (1967)
16. R. J. Briggs J. D. Daughterty, and R. H. Levy, *Phys. Fluids* **13**, 421 (1970)
17. H. P. Furth, *Phys. Fluids* **8**, 2020 (1965)
18. N. C. Christofilos, W. C. Condit, Jr., T. J. Fessenden, R. E. Hester, S. Humphries, G. D. Porter, B. W. Stallard, and P. B. Weiss, *Plasma Phys. and Controlled Nucl. Fusion Research, 1971*, (IAEA, Vienna, 1971), Vol. 1, p. 119
19. W. C. Condit, Jr. and R. V. Lovelace, *Phys. Fluids* **17**, 1719 (1974)
20. G. D. Porter and B. W. Stallard, *Phys. Fluids* **17**, 1722 (1974)
21. R. Prohaska and A. Fisher, *Rev. Sci. Instrum.* **53**, 1092 (1982)
22. H. Ishizuka, G. Leslie, B. Mandelbaum, A. Fisher, and N. Rostoker, *IEEE Trans. Nucl. Sci.* **NS-32**, 2727 (1985)

Downloaded From: http://proceedings.spiedigitallibrary.org/ on 01/14/2015 Terms of Use: http://spiedl.org/terms